

Research Articles: Systems/Circuits

Stimulus Contrast Affects Spatial Integration in the Lateral Geniculate Nucleus of Macaque Monkeys

https://doi.org/10.1523/JNEUROSCI.2946-20.2021

Cite as: J. Neurosci 2021; 10.1523/JNEUROSCI.2946-20.2021

Received: 19 November 2020 Revised: 30 May 2021 Accepted: 2 June 2021

This Early Release article has been peer-reviewed and accepted, but has not been through the composition and copyediting processes. The final version may differ slightly in style or formatting and will contain links to any extended data.

Alerts: Sign up at www.jneurosci.org/alerts to receive customized email alerts when the fully formatted version of this article is published.

Stimulus Contrast Affects Spatial Integration in the Lateral Geniculate Nucleus of Macaque Monkeys

Darlene R. Archer^{1,2,3}, Henry J. Alitto¹, and W. Martin Usrey^{1,*}

¹ Center for Neuroscience, University of California, Davis, CA ² SUNY College of Optometry, New York, NY ³ Center for Neural Science, New York University, New York, NY

Running title: Contrast and spatial integration in the LGN

Abstract: 226 words Significance: 120 words Introduction: 667 words Discussion: 1424 words

Keywords: receptive field, LGN, suppression, extraclassical, gain control

* Correspondence: Center for Neuroscience University of California, Davis 1544 Newton Court Davis, CA 95618 wmusrey@ucdavis.edu

Acknowledgements: We thank K.E. Neverkovec, D.J. Sperka, J.S. Johnson, and R. Oates for expert technical assistance and Dr. Jose-Manuel Alonso for helpful discussions and comments on the manuscript. This work was supported by NIH grants EY013588, MH082174, and P30 EY12576.

ABSTRACT

48

49

50

51

52

53

54

55

56

57

58

59

60

61

62

63

64

65

66

67

68

Gain-control mechanisms adjust neuronal responses to accommodate the wide range of stimulus conditions in the natural environment. Contrast gain control and extraclassical surround suppression are two manifestations of gain control that govern the responses of neurons in the early visual system. Understanding how these two forms of gain control interact has important implications for the detection and discrimination of stimuli across a range of contrast conditions. Here, we report that stimulus contrast affects spatial integration in the lateral geniculate nucleus of alert macaque monkeys (male and female), whereby neurons exhibit a reduction in the strength of extraclassical surround suppression and an expansion in the preferred stimulus size with low-contrast stimuli compared to high-contrast stimuli. Effects were greater for magnocellular neurons than for parvocellular neurons, indicating stream-specific interactions between stimulus contrast and stimulus size. Within the magnocellular pathway, contrast-dependent effects were comparable for ON-center and OFF-center neurons, despite ON neurons having larger receptive fields, less pronounced surround suppression, and more pronounced contrast gain control than OFF neurons. Taken together, these findings suggest that the parallel streams delivering visual information from retina to primary visual cortex, serve not only to broaden the range of signals delivered to cortex, but also to provide a substrate for differential interactions between stimulus contrast and stimulus size that may serve to improve stimulus detection and stimulus discrimination under pathway-specific lower and higher contrast conditions, respectively.

70 **SIGNIFICANCE**

Stimulus contrast is a salient feature of visual scenes. Here we examine the influence of 71 72 stimulus contrast on spatial integration in the lateral geniculate nucleus (LGN). Our 73 results demonstrate that increases in contrast generally increase extraclassical 74 suppression and decrease the size of optimal stimuli, indicating a reduction in the extent of visual space from which LGN neurons integrate signals. Differences between 75 76 magnocellular and parvocellular neurons are noteworthy and further demonstrate that 77 the feedforward parallel pathways to cortex increase the range of information conveyed 78 for downstream cortical processing, a range broadened by diversity in the ON and OFF 79 pathways. These results have important implications for more complex visual 80 processing that underly the detection and discrimination of stimuli under varying natural conditions. 81

INTRODUCTION

82

83

84

85

86

87

88

89

90

91

92

93

94

95

96

97

98

99

100

101

102

103

104

105

106

Visual features in the natural environment vary greatly in luminance contrast and size. To encode these variations efficiently, visual neurons can adjust their responses according to the statistics of the visual scene. Gain-control mechanisms play a prominent role in this process and are evident at every stage in the visual system, often regulating neuronal responses to adjust the sensitivity for stimuli and/or the operating range for processing sensory signals.

Two manifestations of gain control are contrast gain control and extraclassical suppression. Contrast gain control is the phenomenon whereby visual responses are amplified at low contrasts and compressed at high contrasts (Shapley and Victor, 1978; Enroth-Cugell and Freeman, 1987; Victor, 1987; Benardete et al., 1992). Models of retinal mechanisms for contrast gain control often include the combining of linear and nonlinear subunits that dynamically adjust their gain to different contrasts (Shapley and Victor, 1978; Enroth-Cugell and Freeman, 1987; Victor, 1987; Benardete et al., 1992; Chander and Chichilnisky, 2001; Kim and Rieke, 2001). The combination of functional subunits is thought to span a region of visual space that is as large as or larger than a neuron's classical receptive field, thereby potentially contributing to a second form of gain control known as extraclassical suppression (Bonin et al., 2005), a phenomenon in which responses to stimuli within a neuron's classical receptive are suppressed by stimuli within the extraclassical surround (Allman et al., 1985; Sillito et al., 1993; Jones et al., 2000; Solomon et al., 2002, 2006; Alitto and Usrey, 2008; Fisher et al., 2017). As these two manifestations of gain control may include shared (Bonin et al., 2005) and/or distinct retinal mechanisms (Rieke, 2001; Kim and Rieke, 2003; Zaghloul et al., 2007; Jarsky et al., 2011; Weick and Demb, 2011; Greschner et al., 2016), as well as extraretinal mechanisms affecting LGN responses (Sillito et al., 2002; Rathbun et al., 2016; Fisher et al., 2017), it is important to know if and how they interact, as these interactions could have pronounced effects on visual processing.

108

109

110

111

112

113

114

115

116

117

118

119

120

121

122

123

124

125

126

127

128

129

130

131

The effect of stimulus contrast on extraclassical suppression could be distinct for neurons in the parallel retino-geniculo-cortical pathways. In primates, two major pathways from retina to cortex are the magnocellular and parvocellular pathways, which each include ONcenter and OFF-center streams. Compared to neurons in the parvocellular pathway, neurons in the magnocellular pathway have larger receptive fields, shorter visual response latencies, and more transient responses to visual stimuli (reviewed in Schiller and Logothetis, 1990; Merigan and Maunsell, 1993; Usrey and Alitto, 2015). Magnocellular neurons also exhibit greater contrast gain control and stronger extraclassical suppression than parvocellular neurons (Solomon et al., 2002; Alitto and Usrey, 2008). Although contrast gain control and extraclassical suppression are evident in the retinal ganglion cells (RGC) that innervate neurons in the lateral geniculate nucleus (LGN) of the thalamus (Solomon et al., 2006; Alitto and Usrey, 2008), reports indicate these forms of gain control are more pronounced in the LGN compared to the retina (Rathbun et al., 2016; Fisher et al., 2017; but see Alitto and Usrey, 2008). Thus, extraretinal mechanisms may influence interactions between stimulus contrast and stimulus size along the retino-geniculo-cortical pathway, presumably to enhance visual processing in the cortex and benefit visual behavior.

The goal of this study was to assess the influence of stimulus contrast on extraclassical suppression and optimal stimulus size in LGN neurons of alert macaque monkeys to avoid potential confounds associated with anesthesia effects on visual responses (Alitto et al., 2011; Vaiceliunaite et al., 2013) and to determine whether contrast-dependent changes in spatial integration differ for LGN neurons relaying signals in the parallel visual pathways. Across cell-types, the strength of extraclassical suppression typically increased as stimulus contrast increased, and increased suppression was accompanied with shifts in the peak response to smaller optimal-size stimuli, indicating a reduction in the spatial extent over which LGN neurons integrate visual signals. Effects were most pronounced for magnocellular neurons compared to

parvocellular neurons, and differences between ON-center and OFF-center magnocellular
neurons in spatial integration and contrast gain control were noteworthy. Taken together, these
findings demonstrate that stream-specific interactions between stimulus contrast and stimulus
size broaden the range of signals delivered to cortex. Moreover, the inverse relationship
between contrast and spatial integration and the diversity across cell types should have
functional consequences for stimulus detection and discrimination during natural vision.

MATERIALS AND METHODS

indicated in the autocorrelograms.

139

140

141

142

143

144

145

146

147

148

149

150

151

152

153

154

155

156

157

158

159

160

161

162

163

Two adult rhesus monkeys (Macacca mulatta; one female and one male) were used for electrophysiological recordings in this study. All experimental procedures conformed to NIH and USDA guidelines and were approved by the Institutional Animal Care and Use Committee at the University of California, Davis, Under full surgical anesthesia, the monkeys received a cranial implant containing a head post for head stabilization. Animals were then trained to fixate on a target dot for fluid reward while eye position was monitored with an ASL-6 infrared eye tracking system (Applied Science Laboratories, Bedford, MA) with a sampling rate of 1000 Hz. Following fixation training, a stainless-steel recording cylinder (Crist Instruments, Hagerstown, MD) centered over the LGN (7 mm anterior to the interaural axis and 11 mm lateral from the midline) was added to the implant. Electrophysiological recordings and visual stimuli. Single-unit recordings from LGN neurons were made using platinum-in-glass electrodes (1-2 MΩ; Alpha Omega, Alpharetta, GA). Using a microdrive (40 mm MEM, Thomas Recording, Giessen, Germany) mounted on the recording chamber, electrodes were advanced through a stainless-steel guide tube to the LGN, approximately 23 mm below the cortex. Continuous voltage signals containing the action potentials of single units were amplified (A-M Systems, Sequim, WA), filtered (0.1–5 kHz), and recorded using a Micro1401 data acquisition system (28

Visual stimuli were generated with a ViSaGe (Cambridge Research Systems, Rochester, UK) and presented on a gamma-corrected CRT monitor (Sony or Mitsubishi) positioned in front of the animal (at 65 and 80 cm for Monkeys 1 and 2, respectively); the display had a resolution of 1024x768, a refresh rate of 140 Hz or 120 Hz, and a mean luminance of 38 cd/m². At the

kHz) and Spike2 software (CED, Cambridge, UK). Unit isolation was confirmed offline using

waveform analysis and the presence of a refractory period (Bishop and Evans, 1956), as

beginning of each recording session, eye position was calibrated by having the animal fixate target points displayed at known eccentricities. Receptive field locations of recorded neurons were determined manually using small spots and/or grating patches. Visual stimuli were centered on the receptive fields of recorded cells. Importantly, centering was confirmed and maintained throughout data collection. To minimize errors arising from eye movements, trials were aborted if eye position deviated by > 0.35°, and data from trials with broken fixation were discarded.

Visual stimuli appeared after 200 ms of fixation and were presented for 1.5 s during which the animal was required to maintain fixation of a 0.2° target dot centered within a 0.5° radius window for a fluid reward. Individual trials were presented in 3-7 blocks of randomly interleaved stimulus diameters such that each stimulus diameter was presented once during each block. A mean gray interstimulus interval of 1.5 s was interleaved between each stimulus presentation during which animals could move their eyes freely.

We measured responses evoked by drifting sinusoidal gratings (temporal frequency, 4 or 5 Hz) to characterize receptive field response properties. We presented nine spatial frequencies (100% contrast) in octave steps (ranging from 0.2 to 8 c/deg) to characterize the spatial frequency tuning function. From the online spatial frequency response functions, we obtained the frequency that gave the peak response (preferred spatial frequency) and used this spatial frequency for all subsequent stimulus gratings. To measure responses as a function of stimulus size, we presented gratings at nine stimulus diameters (ranging from 0.2°–5°). Contrast response functions were made based on responses to nine luminance contrasts (ranging from 1 to 100% in logarithmic steps). To examine the effect of contrast on extraclassical suppression and optimal stimulus size, we measured size-tuning responses at high and low contrasts.

Data analysis.

- LGN responses were analyzed using the first harmonic (F1) of spiking responses modulated at the temporal frequency of the drifting sinusoidal grating. To find the model parameters that best accounted for the measured responses, a constrained nonlinear least-squares optimization routine, implemented in MATLAB (fmincon), was used when fitting response functions.
- 192 Spatial frequency response functions.
- 193 We fit responses to stimuli that varied in spatial frequency with a frequency domain difference of
- 194 Gaussians (DoG) function (Enroth-Cugell and Robson, 1966) with the following form:

$$R(\omega_x) = K([exp - (\omega_x / f_c)^2] - K_s[exp - (\omega_x / f_s)^2]),$$

- 195 where ω_x is the spatial frequency, K is an overall scaling factor, f_c is the characteristic spatial
- 196 frequency of the center Gaussian (frequency at which the response falls to 1/e of its maximum),
- 197 K_s is the integrated weight of the surround relative to the center, and f_s is the characteristic
- 198 frequency of the surround Gaussian.
- 199 Contrast response functions.
- 200 Contrast response functions were made for a subset of neurons (n = 54). We fit contrast
- 201 responses with a hyperbolic ratio function (Naka and Rushton, 1966; Albrecht and Hamilton,
- 202 1982):

203
$$R(C) = k * C^n/(C^n + C_{50}^n) + b$$

- where C denotes the luminance contrast of the stimulus, k represents the maximum response,
- 205 the exponent n reflects the linearity of the response function, C_{50} refers to the semisaturation
- 206 contrast, and b is the baseline response of the cell. The hyperbolic ratio fits were very good in
- 207 most cases (mean $R^2 = 0.93$).

From the hyperbolic ratio fits, we estimated the contrast required to evoke half of the maximum response (C_{50}), a value which reflects the slope of the contrast response function, and we used this measure to quantify the contrast gain for a given cell.

To examine extraclassical suppression and optimal stimulus size across neurons, we selected contrast levels above and below each cell's C_{50} in the linear range of the contrast response function (typically the C_{25} and C_{75} , assessed online) to generate area summation response functions.

215 Size-tuning response functions.

208

209

210

211

212

213

- 216 We fit responses to stimulus diameter with a spatial domain difference of Gaussians (DOG)
- 217 function (Sceniak et al., 1999) with the following form:

218
$$R(d) = K_c \int_{-d/2}^{d/2} \exp(-[2y/\sigma_c]^2) - K_s \int_{-d/2}^{d/2} \exp(-[2y/\sigma_s]^2),$$

- where d is the stimulus diameter in degrees, K_c and σ_c specify the amplitude and width of the center Gaussian, and K_s and σ_s specify the amplitude and width of the surround Gaussian. The only constraint imposed when fitting the data was $\sigma_c < \sigma_s$.
- From the DoG fits, we obtained the peak response and asymptotic response to estimate
 the degree in which the extraclassical surround modulates the response of the classical center
 (DeAngelis et al., 1994). Using these measures, we calculated the suppression index (SI),
 defined as follows:

$$SI = (R_{peak} - R_{asym})/(R_{peak} + R_{asym}),$$

- where R_{peak} reflects the maximum response across all stimulus diameters, and R_{asym} reflects the asymptotic response to the largest stimulus diameter. SI values are bound between 0 and 1:
- 229 with values near 0 representing weak suppression, and larger values representing strong

252

230 suppression. We obtained the stimulus diameter eliciting the peak response to estimate the 231 optimal stimulus size, a value that approximates the size of the classical receptive field. 232 Changes in the optimal stimulus size as a function of contrast were quantified using a bounded 233 index: $(Opt.size_{low\;contrast}\;-\;Opt.size_{high\;contrast}\,)/(Opt.size_{low\;contrast}\;+\;Opt.size_{high\;contrast})$ 234 Cell classification. 235 We classified cells as magnocellular or parvocellular using clustering analysis in Matlab. 236 Hierarchical clustering performed a weighted linkage algorithm based on the contrast evoking 237 half-maximum response (C₅₀) and the slope of the contrast response function for lower 238 contrasts (1.8% to 17.8%). Consistent with our previous findings (Alitto and Usrey, 2008), this 239 method generated clusters where cells with a C₅₀ < 35% were classified as magnocellular (n = 240 35) and cells with a $C_{50} > 35\%$ were classified as parvocellular (n = 19). Because recording sites 241 were not confirmed with lesions and histology (not a feasible practice for data collected from 242 behaving animals), we consider the classification of cell types as putative magnocellular and 243 putative parvocellular. 244 Cells were further classified as ON-center or OFF-center based on their response to the 245 phase of the sinusoidal grating. Cells excited by the bright phase of the stimulus were classified 246 as ON cells, and cells excited by the dark phase were classified as OFF cells. Given the smaller 247 number of parvocellular cells (n = 19, total) did not allow for significant statistical analysis, we 248 restricted the ON-OFF analysis to our sample of magnocellular cells, as we had a sufficient 249 sample size of both cell types (n = 19 and n = 16 for OFF and ON cells, respectively). 250 Statistics.

nonparametric Wilcoxon signed-rank test (MATLAB function: signrank) was used to evaluate the

All analyses were performed using built-in MATLAB functions and custom scripts. The

effect of stimulus contrast within a single cell and determine p values for all pair-wise statistical tests. The nonparametric Wilcoxon rank sum test (MATLAB function: ranksum) was used to compare measures of SI, optimal size, C_{50} , response gain, and contrast-dependent changes between cell-type groups and determine p values for statistical tests.

A Spearman (rank) correlation coefficient (MATLAB function: *corr*) was calculated to quantify the relationship between measures of interest and determine significance. From correlations, we calculated a Spearman (rank) partial correlation coefficient (MATLAB function: *partialcorr*) as follows:

261
$$r_{xy.z} = (r_{xy} - r_{xz}r_{yz}) / \sqrt{(1 - r_{xz}^2)(1 - r_{yz}^2)}$$

to confirm the relationship between two measures of interest (x, y) while controlling for the effect of a third measure (z) and determine significance.

For all comparisons, the mean and the standard error of the mean (SEM) are reported, and the number of neurons in each group is presented as values for n. Probability values are provided for all statistical comparisons, and probability values smaller than 0.001 are described as p < 0.001. All statistical methods were two-sided.

RESULTS

268

269

270

271

272

273

274

275

276

277

278

279

280

281

282

283

284

285

286

287

288

289

290

291

Stimulus contrast and stimulus size are known to govern the responses of neurons in the lateral geniculate nucleus (LGN) and, therefore, the visual signals relayed to cortex. We made single-unit recordings from neurons (n = 75) in the LGN of 2 awake, fixating macaque monkeys to determine how these stimulus features interact. For each neuron, we measured responses to drifting sinusoidal gratings (optimal spatial frequency; temporal frequency, 4 or 5 Hz), that were centered over the receptive field and varied in contrast and size (i.e., diameter of the grating patch).

Figure 1A and B shows the spiking activity and firing rates of an example LGN neuron for stimuli of different contrasts and sizes. The periodic spiking activity in the raster plots (Fig. 1A) reflects the phase and temporal frequency of the drifting sinusoidal grating. As expected, the spiking activity of this neuron increases as stimulus contrast increases (5%, 8%, and 18% contrast). Activity levels of this neuron are also affected by stimulus size, as illustrated with each of the response curves in Figure 1B. Beginning with the smallest size stimuli, the initial increase in the response function largely reflects the extent to which the stimulus fills the classical receptive field of the neuron. The peak response (arrowheads) corresponds to the optimal stimulus size, a value that approximates the size of the classical receptive field and marks the border for response reinforcement, i.e., spatial integration (see Materials and Methods). Consistent with the view that the extraclassical receptive field overlaps and extends beyond the classical receptive field, stimulus sizes larger than the optimal size suppress the firing rate of the neuron as suppression increases at a faster pace than excitation until a plateau response is reached, at which point the stimulus extends beyond the size of the extraclassical surround. This example neuron exhibits substantial extraclassical suppression for higher contrast stimuli (18% contrast) and less suppression for lower contrast stimuli (5% contrast). Additionally, the

293

294

295

296

297

298

299

300

301

302

303

304

305

306

307

308

309

310

311

312

313

314

315

316

rightward shift in the size-tuning response curves with lower contrasts reveals an inverse relationship between stimulus contrast and preferred stimulus size.

To examine the effect of contrast on extraclassical surround suppression across the sample of LGN neurons, we calculated a bounded suppression index (SI; the difference between the peak response and asymptote response divided by the sum of these responses; Fig. 1C; see Materials and Methods). For the example LGN neuron in Figure 1, increases in stimulus contrast increased the cell's peak response (Fig. 1D), decreased the optimal size for peak response (Fig. 1E), and increased the suppression index (Fig. 1F).

Similar to the example neuron in Figure 1, contrast had a prounounced influence on extraclassical suppression (Fig. 2A) and size tuning (Fig. 2B) across our sample of LGN neurons (n = 75). Using a wide range of stimulus contrasts (mean high contrast used = 54.9% ± 3.9%; mean low contrast used = 17.7% ± 1.6%), the SI was significantly increased as the stimulus contrast was increased (Wilcoxon signed-rank test; p < 0.001). Overall, suppression indices were ~44% greater for stimuli at higher contrasts (mean SI: 0.23 ± 0.01) compared to lower contrasts (mean SI: 0.16 ± 0.01 ; p < 0.001, Wilcoxon rank sum test). Stimulus contrast also affected the size of the preferred stimulus. Across LGN neurons, optimal sizes were ~20% larger for stimuli at lower contrasts (mean optimal size: 0.96° ± 0.04°) compared with higher contrasts (mean optimal size: 0.80° ± 0.04°, p = 0.004, Wilcoxon rank sum test). Taken together, the increase in optimal stimulus size and the reduction in extraclassical suppression are consistent with results from cortical neurons showing an increase in the extent of spatial integration at low contrast compared with high contrast (Levitt and Lund, 1997; Kapadia et al., 1999; Sceniak et al., 1999; Shushruth et al., 2009); however, not all cells displayed similar effects from contrast, we therefore examined the influence of stimulus contrast on a subset of LGN neurons in our sample with clear cell-class identity (below).

Magnocellular and parvocellular responses to stimulus contrast

318

319

320

321

322

323

324

325

326

327

328

329

330

331

332

333

334

335

336

337

338

339

340

Magnocellular and parvocellular LGN neurons have distinct response profiles for stimuli that vary in stimulus contrast (Reviewed in Schiller and Logothetis, 1990; Merigan and Maunsell, 1993). Figure 3 shows the contrast response functions of an example parvocellular and magnocellular neuron. As is typical for these cell types, the magnocellular neuron is more sensitive to low-contrast stimuli compared to the parvocellular neuron. For the example magnocellular neuron (Fig. 3A), response rates increase relatively linearly over a contrast range of ~2 - 25%, at which point, responses begin to saturate. The contrast required to evoke half of the cell's maximum response (C_{50}) is approximately 13%. For the parvocellular neuron (Fig. 3B), response rates are substantially more linear over a broader range, from ~15 – 80% contrast, and the C₅₀ is higher, approximately 38%. In the following sections we examine the influence of stimulus contrast on extraclassical suppression and optimal size for a subset of neurons that were identified as magnocellular (n = 35) or parvocellular (n = 19; see Materials and Methods). For each neuron, we determined the contrast levels within the linear range of the responses, and we selected contrasts near the high and low ends of this range (above and below the C50; assessed online) for subsequent evaluation of contrast-dependent changes between cell types. Contrast-dependent effects on suppression and optimal size are greater in magnocellular neurons than in parvocellular neurons As an initial analysis, we compared the strength of extraclassical suppression between magnocellular and parvocellular neurons. Magnocellular neurons displayed significantly stronger extraclassical suppression than parvocellular neurons when shown higher contrast stimuli (Fig. 4A; p = 0.003, Wilcoxon rank sum test). A similar relationship was also evident with lower contrast stimuli; however, the difference between magnocellular and parvocellular neurons did not reach significance (Fig. 4A; p = 0.09, Wilcoxon rank sum test). Thus, cell-type

differences in extraclassical suppression were contingent on contrast.

342

343

344

345

346

347

348

349

350

351

352

353

354

355

356

357

358

359

360

361

362

363

Among magnocellular neurons, suppression indices were ~60% greater for stimuli at higher contrast than at lower contrast (Fig. 4B; mean SI: high contrast = 0.29 ± 0.02; low contrast = 0.18 ± 0.01 ; p < 0.001, Wilcoxon rank sum test; mean high contrast used = $27.0\% \pm 0.001$ 2.7%, mean effective contrast (i.e. % of maximum response) = $71.3\% \pm 2.2\%$); mean low contrast used = $9.0\% \pm 0.7\%$, mean effective contrast = $37.4\% \pm 2.3\%$). This effect was typical of magnocellular neurons, with 91% (32 of 35) of magnocellular neurons showing an increase in surround suppression at higher contrasts compared to lower contrasts (p < 0.001, Wilcoxon signed rank test). For the parvocellular neurons in our sample, we did not see a significant influence of stimulus contrast on extraclassical suppression (Fig. 4C; mean SI: high contrast = 0.19 ± 0.02 ; low contrast = 0.16 ± 0.04 ; p = 0.13, Wilcoxon signed-rank test; mean high contrast used = $56.5\% \pm 3.6\%$, mean effective contrast = $60.5\% \pm 4.3\%$; mean low contrast used = 30.8% \pm 2.9%, mean effective contrast = 17.1% \pm 3.5%); however, we cannot rule out the possibility that a significant, albeit small, difference might have been detected with a larger sample size. Nevertheless, compared to parvocellular neurons (mean change in $SI = 0.03 \pm$ 0.02), magnocellular neurons (mean change in SI = 0.11 ± 0.02) had a significantly greater contrast-dependent effect on extraclassical surround suppression (Fig. 4D; p = 0.001, Wilcoxon rank sum test).

We also observed differences between magnocellular and parvocellular neurons when comparing optimal stimulus size. With lower contrast stimuli, magnocellular neurons preferred significantly larger stimuli than did parvocellular neurons (Fig. 4E; p < 0.001, Wilcoxon rank sum test). Notably, this difference was not significant in response to higher-contrast stimuli (Fig. 4E; p = 0.13, Wilcoxon rank sum test). Thus, cell-type differences in optimal stimulus size also depended on contrast.

Among the magnocellular neurons, optimal sizes were ~28% larger for lower-contrast
stimuli compared to higher-contrast stimuli (Fig. 4F; mean optimal size: low contrast = $1.10^{\circ} \pm$
0.06°; high contrast = 0.86° \pm 0.05°, respectively; p = 0.006, Wilcoxon rank sum test). This effects
was typical for magnocellular neurons, with 91% (32 of 35) of magnocellular neurons showing
an expansion in optimal stimulus size at lower contrasts compared to higher contrasts ($p <$
0.001, Wilcoxon signed-rank test). As with cell-type-specific differences in extraclassical
suppression, stimulus contrast did not have a significant effect on optimal stimulus size for the
parvocellular neurons in our sample (Fig. 4G; mean optimal size: low contrast = $0.78^{\circ} \pm 0.06^{\circ}$;
high contrast = $0.73^{\circ} \pm 0.06^{\circ}$; $p = 0.15$, Wilcoxon signed-rank test). Thus, compared to
parvocellular neurons (mean change for optimal size = $0.05^{\circ} \pm 0.03^{\circ}$; bounded index = $0.03 \pm 0.03^{\circ}$
0.02; see Materials and Methods), magnocellular neurons (mean change for optimal size =
$0.24^{\circ} \pm 0.03^{\circ}$; bounded index = 0.14 ± 0.02 ; see Materials and Methods) exhibited significantly
greater contrast-dependent changes in the spatial extent of the receptive field (Fig. 4H; $p =$
0.001, Wilcoxon rank sum test).
ON-OFF asymmetries in spatial integration and contrast gain control for cells in the
magnocellular pathway
Together, these results show that magnocellular, but not parvocellular neurons exhibit contrast-
dependent changes in spatial integration, and spatial asymmetries between magnocellular and
parvocellular neurons were contingent on contrast. In the sections below, we examine whether
these effects of contrast further differentiate for the ON and OFF streams within the
magnocellular pathway.
We first compared extraclassical suppression between our sample of ON-center and
OFF-center magnocellular neurons (n = 16 and n = 19, respectively). Comparisons revealed a
significant difference for higher-contrast stimuli (Fig. 5A; mean SI: OFF cells = 0.33 ± 0.03 ; ON

cells = 0.24 \pm 0.01; p = 0.006, Wilcoxon rank sum test), although the difference did not quite

390

391

392

393

394

395

396

397

398

399

400

401

402

403

404

405

406

407

408

409

410

411

412

413

reach significance for lower contrast stimuli (mean SI: OFF cells = 0.20 ± 0.02 ; ON cells = 0.15 ± 0.01 ; p = 0.10, Wilcoxon rank sum test). Nevertheless, for both the ON cells and the OFF cells, extraclassical suppression significantly increased in response to higher-contrast stimuli compared with lower contrast stimuli (Fig. 5B; p < 0.001, Wilcoxon signed-rank test), and the contrast-dependent changes in suppression indices between the two cell types were not significantly different (Fig. 5C; mean change SI: ON cells = 0.09 ± 0.01 ; OFF cells = 0.13 ± 0.03 ; p = 0.23, Wilcoxon rank sum test).

Previous studies have reported asymmetries in the size of receptive fields between ON and OFF cells in the macaque retina, with ON cells having larger receptive fields (Chichilnisky and Kalmar, 2002; see Ravi et al., 2018). Thus, we next compared optimal stimulus size between our sample of ON-center and the OFF-center magnocellular neurons. We found that optimal sizes were larger for ON cells than OFF cells, regardless of contrast, as these differences were significant for both the higher contrast stimuli (Fig. 5D; mean optimal size: ON cells = $1.03^{\circ} \pm 0.07^{\circ}$; OFF cells = $0.72^{\circ} \pm 0.07^{\circ}$; p = 0.003, Wilcoxon rank sum test; mean effective contrast (i.e. % of maximal response) used for comparison: ON cells = 71.5% ± 2.3%; Off cells, 71.1% ± 3.7%; p = 0.68, Wilcoxon rank sum test) and the lower contrast stimuli (Fig. 5D; mean optimal size: ON cells = $1.30^{\circ} \pm 0.09^{\circ}$; OFF cells = $0.93^{\circ} \pm 0.06^{\circ}$; p = 0.001, Wilcoxon rank sum test; mean contrast used for comparison = ON cells, 8.4% ± 1.2%; OFF cells, 9.5% ± 0.8%; p = 0.17, Wilcoxon rank sum test). Furthermore, both ON and OFF cells exhibited significant increases in optimal stimulus size in response to lower contrast stimuli compared with higher contrast stimuli (Fig. 5E; p < 0.001, Wilcoxon signed-rank test), and the contrastdependent changes were not significantly different for the two types of cells (Fig. 5F; p = 0.56, Wilcoxon rank sum test). Thus, these comparisons in extraclassical suppression strength and optimal stimulus size suggest that there are notable differences in spatial integration between ON and OFF magnocellular neurons.

Because receptive-field size is known to increase with eccentricity (Derrington and Lennie, 1984; Croner and Kaplan, 1995; Kremers and Weiss, 1997; Usrey and Reid, 2000; Solomon et al., 2002), we next tested whether these ON-OFF differences in optimal stimulus size observed in our sample of magnocellular neurons might be due to sampling differentially from cells at small and large eccentricities. As shown in Figure 6, optimal size indeed increased as a function of receptive-field eccentricity across magnocellular cells (r = 0.59, p < 0.001), an effect evident for both the ON cells (r = 0.51, p = 0.003) and the OFF cells (r = 0.49, p = 0.002); however, the pool of ON cells did not differ significantly from the OFF cells in their eccentricity (p = 0.18, Wilcoxon rank sum test). More importantly, at any given eccentricity optimal size was, on average, larger for ON cells compared to OFF cells. Similar to the results obtained in the retina (Chichilnisky and Kalmar, 2002), across our sample of LGN magnocellular neurons, ON cells preferred larger size stimuli than OFF cells.

We next asked how features of spatial integration are related to each other. To address this question, we compared suppression-index values and optimal-stimulus sizes across our sample of ON and OFF magnocellular neurons. As shown in Figure 7A, there was a negative correlation between these two values (r = -0.46, p < 0.001; ON cells: r = -0.43, p = 0.01; OFF cells: r = -0.35, p = 0.03). That is, cells that preferred smaller stimuli typically exhibited stronger extraclassical suppression compared with cells that preferred larger stimuli. To confirm the relationship between surround suppression (SI) and optimal size (RF), we computed an optimal size partial correlation while controlling for C_{50} ($r_{SIRF,C50} = -0.40$, p < 0.001). Together, these results suggest that ON cells integrate signals over larger regions of visual space compared with OFF cells.

Previous studies in the macaque retina have also noted ON-OFF asymmetries in contrast response functions, with ON cells showing higher contrast sensitivity (Chander and Chichilnisky, 2001; Chichilnisky and Kalmar, 2002). To test whether these asymmetries are also

present in the macaque LGN, we compared contrast gain control between ON and OFF magnocellular neurons using the C_{50} as a measure for contrast gain control (the lower the C_{50} , the greater the contrast gain control). As illustrated in Figure 7B, C_{50} values were significantly lower for ON cells compared with OFF cells (mean C_{50} : ON cells = 10.6% \pm 1.1%; OFF cells = 21.8% \pm 1.3%; p < 0.001, Wilcoxon rank sum test), indicating ON magnocellular cells exhibit more pronounced contrast gain control compared with OFF magnocellular cells.

Given the differences in spatial integration and contrast gain control that we observed for magnocellular ON and OFF cells, we tested whether variations in the contrast-dependent strength of surround suppression correlated with the distribution of C_{50} values. As shown in Figure 7C, there was a positive correlation between these two values (r = 0.39, p < 0.001), indicating an inverse relationship between these forms of gain control. That is, cells with higher suppression indices (stronger surround suppression) had higher C_{50} values (less contrast gain control). Thus, cells in the magnocellular pathway that exhibited stronger surround suppression exhibited less pronounced contrast gain control. Moreover, controlling for optimal stimulus size (RF) did not lower the strength of the relationship between extraclassical suppression (SI) and C_{50} by that much when we computed a partial correlation ($r_{SIC50.RF} = 0.35$, p = 0.003, see Methods), indicating optimal stimulus size does not account for the inverse relationship. Taken together, these findings indicate manifestations of gain-control mechanisms that regulate neuronal responsiveness in the macaque LGN differentiate between the ON and OFF streams within the magnocellular pathway.

DISCUSSION

Our results demonstrate spatial integration in LGN neurons is regulated in a contrast-dependent manner and differentiates across parallel visual pathways – having implications for downstream visual processing and perception (Nirenberg et al., 2010; Jiang et al., 2015). Most LGN neurons exhibited an increase in extraclassical suppression strength and a constriction in the optimal stimulus size in response to higher contrast stimuli, indicating a reduction in spatial integration, as reported for V1 neurons (Levitt and Lund, 1997; Kapadia et al., 1999; Sceniak et al., 1999; Shushruth et al., 2009). Some neurons, notably those in the parvocellular pathway, did not exhibit these changes with contrast. Within the magnocellular pathway, ON and OFF neurons exhibited similar changes with contrast, despite ON neurons exhibiting broader spatial integration than OFF neurons. These findings demonstrate that the spatial dimensions of geniculate receptive fields are dynamic and support the notion that stimulus-evoked changes in the integration field are due to shifts in the balance between excitation and inhibition (Levitt and Lund, 1997; Kapadia et al., 1999; Cavanaugh et al., 2002); thus, providing a way for the visual system to adjust the extent of spatial integration needed to accommodate for changes in the visual environment.

Previous studies reported extraclassical suppression in the retina is stronger for magnocellular-projecting compared to parvocellular-projecting RGCs (Solomon et al., 2006; Alitto and Usrey, 2008). Moreover, among magnocellular-projecting RGCs, contrast affects both surround suppression and optimal stimulus size (Solomon et al., 2006). Our results from LGN neurons therefore presumably include a retinal contribution; however, extraretinal mechanisms are also indicated, as extraclassical suppression and contrast gain control are augmented in the LGN (Rathbun et al., 2016; Fisher et al., 2017; but see Alitto and Usrey, 2008). Thus, mechanisms underlying the dynamic changes between excitation and inhibition likely rely on

485

486

487

488

489

490

491

492

493

494

495

496

497

498

499

500

501

502

503

504

505

506

507

508

multiple circuits, including input from the retina, thalamic inhibition, and feedback from primary visual cortex (V1).

LGN relay cells integrate driving input that is stream-specific from RGCs and modulatory inputs from a variety of feedforward and feedback sources. Feedback from V1 provides extensive modulatory input to the LGN that aligns with the feedforward parallel pathways (Briggs and Usrey, 2009). Synapses from corticogeniculate neurons are glutamatergic; however, their associated EPSPs are smaller compared with those from RGCs (Bloomfield and Sherman, 1988; Paulsen and Heggelund, 1994; Granseth and Lindström, 2003). The corticogeniculate feedback pathway also includes disynaptic inhibition onto relay cells, via local interneurons (Wilson, 1989) and neurons in the thalamic reticular nucleus (TRN; Bragg et al., 2017). Inactivation studies indicate a role for corticogeniculate feedback in extraclassical suppression (Murphy and Sillito, 1987; Sillito and Jones, 2002; Andolina et al., 2013) and support the idea that feedback may contribute to contrast-dependent modulation of size-tuning in the LGN (Sceniak et al., 2006). Importantly, local interneurons integrate retinal and corticogeniculate inputs, whereas TRN neurons integrate geniculocortical and corticogeniculate inputs; thereby providing the opportunity for gain modulation to occur in a feedforward and/or feedback manner (Vaingankar et al., 2012; Soto-Sanchez et al., 2017). The influence of extraretinal mechanisms also depends on where synapses are made on the dendrites of relay cells. RGCs and LGN interneurons preferentially target proximal dendrites (Wilson, 1989), corticogeniculate cells target distal dendrites (Wilson, 1989), and TRN neurons target both proximal and distal dendrites with a preference for more distal dendrites (Cucchiaro et al., 1991; Wang et al., 2001). Taken together, the different sources for inhibition and segregation of synaptic inputs onto different dendritic regions provide an opportunity for dynamic postsynaptic interactions. Although the details of these interactions remain undetermined, our results suggest they occur in a stream-specific fashion.

Our results demonstrate diversity in the spatial extent over which magnocellular and parvocellular neurons integrate visual signals. At high contrast, magnocellular neurons exhibited stronger extraclassical suppression and comparable optimal stimulus sizes with parvocellular neurons, whereas at low contrast, magnocellular neurons preferred larger stimulus sizes and comparable extraclassical suppression with parvocellular neurons. Under lower contrasts, our results support the generally accepted view that magnocellular neurons have larger receptive fields than parvocellular neurons. Interestingly, some past studies using high-contrast stimuli reported no differences between magnocellular and parvocellular neurons in receptive-field size (Levitt et al., 2001), consistent with our results under higher contrasts. Taken together, results from this study demonstrate magnocellular neurons integrate over a larger visual field than parvocellular neurons at lower contrasts, but not higher contrasts.

To facilitate comparisons between magnocellular and parvocellular neurons, we selected contrast levels within the linear portion of the cell's contrast-response function. Our goal was to use contrast levels that would generate relatively similar responses (with respect to each cell's maximum response) across cells; however, the effective contrasts selected (i.e. % of maximum response) for the low-contrast condition was higher for the magnocellular neurons. With this incongruity noted, it seems unlikely the difference in effective contrasts would account for the contrast-dependent spatial asymmetries we observed between magnocellular and parvocellular neurons, because magnocellular neurons exhibited a larger, not smaller, dynamic range in spatial integration than parvocellular neurons.

Comparisons between magnocellular ON and OFF neurons uncovered differences in surround suppression and receptive-field size indicating ON neurons integrate over a larger visual field than OFF neurons regardless of contrast. The ON and OFF pathways are established in the retina and separately convey increments and decrements in light intensity to cortex (Werblin and Dowling, 1969; Schiller et al., 1986; Schiller, 1992). The ON and OFF pathways extend the dynamic range of operation and are generally considered symmetric

systems that are opposite in sign. Nevertheless, ON-OFF asymmetries in dendritic-field size (Peichl et al., 1987; Peichl, 1989; Tauchi et al., 1992; Manookin et al., 2008; Ratliffe et al., 2010), receptive-field size (Chichilnisky and Kalmar, 2002; Ravi et al., 2018), contrast sensitivity (Chander and Chichilnisky, 2001; Chichilnisky and Kalmar, 2002; Zaghloul et al., 2003), spatial integration (Turner and Rieke, 2016; Ravi et al., 2018), and temporal integration (Chichilnisky and Kalmar, 2002; Pandarinath et al., 2010; Ravi et al., 2018) have been reported in the retina for a range of species, suggesting these functional differences are optimized for encoding sensory information efficiently (Gjorgjieva et al., 2014). The ON-OFF asymmetries in spatial integration reported here for LGN neurons may also influence the capacity for encoding global and local features in a visual scene, as reported for V1 responses to lights and darks (Mazade et al., 2019).

Diversity in the expression of gain control across ON and OFF magnocellular neurons may also be optimal for encoding and integrating a range of visual signals efficiently (Zaghloul et al., 2003; Nirenberg et al., 2010). Contrast gain control amplifies response gain at low contrast – optimizing signal-to-noise and reducing the loss of weak signals; at high contrast, response gain is compressed and integration time is shortened – protecting against saturation (Shapley and Victor, 1978, 1981; Victor, 1987). Thus, neurons expressing more pronounced contrast gain control should exhibit shorter integration times. Moreover, given previous studies have reported an inverse relationship between temporal integration and spatial integration (Frishman et al., 1987; Lee, 1996; Troy and Shou, 2002; Alitto and Usrey, 2015) – a shorter integration time implies larger spatial integration (Ravi et al., 2018) – neurons exhibiting more pronounced contrast gain control should also exhibit larger spatial integration. This prediction is consistent with the differences reported here for magnocellular neurons; ON neurons exhibited larger spatial integration and more pronounced contrast gain control than OFF neurons. Together, these results suggest differences in the expression of gain control across parallel visual pathways in the macaque LGN reflect how the visual system exploits functional

asymmetries, thereby extending the dynamic range of operation to compensate for limitations in signaling capacity and to optimize visual encoding (Nirenberg et al., 2010).

Gain-control mechanisms operate at every stage in the visual system and adjust how visual neurons respond to different stimulus conditions in the natural environment. Similar to how the pupil constricts in response to light and dilates in response to dark, the spatial extent of the receptive field is dynamic, exhibiting constriction and expansion in response to changes in stimulus contrast. These dynamic changes likely optimize the capacity to integrate a range of visual signals and have perceptual consequences. At lower contrasts, expansion of the receptive field and less pronounced surround suppression enhance sensitivity as signals are integrated over larger regions of visual space, thus providing a substrate for improved stimulus detection. Whereas at higher contrasts, constriction of the receptive field and more pronounced surround suppression sharpens spatial boundaries, thus providing a substrate for improved stimulus discrimination. Taken together, these findings suggest diversity across the parallel visual pathways provides a functional benefit for downstream visual processing and perception by optimizing transmission of information about a visual scene in an efficient manner.

576	References
577	Albrecht DG, Hamilton DB (1982) Striate cortex of monkey and cat: contrast response function.
578	J Neurophysiol 48:217–237.
579	Alitto HJ, Moore BD, Rathbun DL, Usrey WM (2011) A comparison of visual responses in the
580	lateral geniculate nucleus of alert and anaesthetized macaque monkeys. J Physiol (Lond)
581	589:87–99.
582	Alitto HJ, Usrey WM (2008) Origin and dynamics of extraclassical suppression in the lateral
583	geniculate nucleus of the macaque monkey. Neuron 57:135–146.
584	Alitto HJ, Usrey WM (2015) Surround suppression and temporal processing of visual signals. J
585	Neurophysiol 113:2605–2617.
586	Allman J, Miezin F, McGuinness E (1985) Stimulus specific responses from beyond the
587	classical receptive field: neurophysiological mechanisms for local-global comparisons in
588	visual neurons. Annu Rev Neurosci 8:407–430.
589	Andolina IM, Jones HE, Sillito AM (2013) Effects of cortical feedback on the spatial properties of
590	relay cells in the lateral geniculate nucleus. J Neurophysiol 109:889-899.
591	Benardete EA, Kaplan E, Knight BW (1992) Contrast gain control in the primate retina: P cells
592	are not X-like, some M cells are. Vis Neurosci 8:483-486.
593	Bishop PO, Evans WA (1956) The refractory period of the sensory synapses of the lateral
594	geniculate nucleus. J Physiol 134:538–557.
595	Bloomfield SA, Sherman SM (1988) Postsynaptic potentials recorded in neurons of the cat's
596	lateral geniculate nucleus following electrical stimulation of the optic chiasm. J
597	Neurophysiol 60:1924–1945.
598	Bonin V, Mante V, Carandini M (2005) The suppressive field of neurons in lateral geniculate
599	nucleus. J Neurosci 25:10844–10856.

600	Bragg EM, Fairless EA, Liu S, Briggs F (2017) Morphology of Visual Sector Thalamic Reticular
601	Neurons in the Macaque Monkey Suggests Retinotopically Specialized, Parallel Stream-
602	Mixed Input to the Lateral Geniculate Nucleus. J Comp Neurol 525:1273–1290.
603	Briggs F, Usrey WM (2009) Parallel processing in the corticogeniculate pathway of the macaque
604	monkey. Neuron 62:135–146.
605	Cavanaugh JR, Bair W, Movshon JA (2002) Nature and interaction of signals from the receptive
606	field center and surround in macaque v1 neurons. J Neurophysiol 88:2530–2546.
607	Chander D, Chichilnisky EJ (2001) Adaptation to temporal contrast in primate and salamander
608	retina. J Neurosci 21:9904–9916.
609	Chichilnisky EJ, Kalmar RS (2002) Functional asymmetries in ON and OFF ganglion cells of
610	primate retina. J Neurosci 22:2737–2747.
611	Croner LJ, Kaplan E (1995) Receptive fields of P and M ganglion cells across the primate retina.
612	Vision Res 35:7–24.
613	Cucchiaro JB, Uhlrich DJ, Sherman SM (1991) Electron-microscopic analysis of synaptic input
614	from the perigeniculate nucleus to the A-laminae of the lateral geniculate nucleus in cats. J
615	Comp Neurol 310:316–336.
616	DeAngelis GC, Freeman RD, Ohzawa I (1994) Length and width tuning of neurons in the cat's
617	primary visual cortex. J Neurophysiol 71:347–374.
618	Derrington AM, Lennie P (1984) Spatial and temporal contrast sensitivities of neurones in lateral
619	geniculate nucleus of macaque. J Physiol 357:219–240.
620	Enroth-Cugell C, Freeman AW (1987) The receptive-field spatial structure of cat retinal Y cells.
621	J Physiol 384:49–79.
622	Enroth-Cugell C, Robson JG (1966) The contrast sensitivity of retinal ganglion cells of the cat. J
623	Physiol 187:517–552.
624	Fisher TG, Alitto HJ, Usrey WM (2017) Retinal and nonretinal contributions to extraclassical
625	surround suppression in the lateral geniculate nucleus. J Neurosci 37:226–235.

626	Frishman L, Freeman A, Troy J, Schweitzer-Tong D, Enroth-Cugell C (1987) Spatiotemporal
627	frequency responses of cat retinal ganglion cells. J Gen Physiol 89:599-628.
628	Gjorgjieva J, Sompolinsky H, Meister M (2014) Benefits of pathway splitting in sensory coding. J
629	Neurosci 34:12127–12144.
630	Granseth B, Lindström S (2003) Unitary EPSCs of Corticogeniculate Fibers in the Rat Dorsal
631	Lateral Geniculate Nucleus In Vitro. J Neurophysiol 89:2952–2960.
632	Greschner M, Heitman AK, Field GD, Li PH, Ahn D, Sher A, Litke AM, Chichilnisky EJ (2016)
633	Identification of a Retinal Circuit for Recurrent Suppression Using Indirect Electrical
634	Imaging. Curr Biol 26:1935-1942.
635	Jarsky T, Cembrowski M, Logan SM, Kath WL, Riecke H, Demb JB, Singer JH (2011) A
636	synaptic mechanism for retinal adaptation to luminance and contrast. J Neurosci 31:11003-
637	11015.
638	Jiang Y, Purushothaman G, Casagrande VA (2015) The functional asymmetry of ON and OFF
639	channels in the perception of contrast. J Neurophysiol 114:2816–2829.
640	Jones HE, Andolina IM, Oakely NM, Murphy PC, Sillito AM (2000) Spatial summation in lateral
641	geniculate nucleus and visual cortex. Exp Brain Res 135:279–284.
642	Kapadia MK, Westheimer G, Gilbert CD (1999) Dynamics of spatial summation in primary visual
643	cortex of alert monkeys. PNAS 96:12073–12078.
644	Kaplan E, Shapley RM (1982) X and Y cells in the lateral geniculate nucleus of macaque
645	monkeys. J Physiol 330:125–143.
646	Kim KJ, Rieke F (2001) Temporal contrast adaptation in the input and output signals of
647	salamander retinal ganglion cells. J Neurosci 21:287–299.
648	Kim KJ, Rieke F (2003) Temporal contrast adaptation in the input and output signals of
649	salamander retinal ganglion cells. J Neurosci 21:287-299.
650	Kremers J, Weiss S (1997) Receptive field dimensions of lateral geniculate cells in the common
651	marmoset (Callithrix jacchus). Vision Res 37:2171–2181.

652 653	Lee BB (1996) Receptive field structure in the primate retina. Vision Res 36:631–644.
654	Levitt JB, Lund JS (1997) Contrast dependence of contextual effects in primate visual cortex.
655	Nature 387:73–76.
656	Levitt JB, Schumer RA, Sherman SM, Spear PD, Movshon JA (2001) Visual response
657	properties of neurons in the LGN of normally reared and visually deprived Macaque
658	monkeys. J Neurophysiol 85:2111–2129.
659	Manookin MB, Beaudoin DL, Ernst ZR, Flagel LJ, Demb JB (2008) Disinhibition combines with
660	excitation to extend the operating range of the OFF visual pathway in daylight. J Neurosci
661	28:4136–4150.
662	Mazade R, Jin J, Pons C, Alonso J-M (2019) Functional Specialization of ON and OFF Cortical
663	Pathways for Global-Slow and Local-Fast Vision. Cell Reports 27:2881-2894.e5.
664	Merigan WH, Maunsell JHR (1993) How parallel are the primate visual pathways? Annu Rev
665	Neurosci:369-402.
666	Murphy PC, Sillito AM (1987) Corticofugal feedback influences the generation of length tuning in
667	the visual pathway. Nature 329:727–729.
668	Naka KI, Rushton WAH (1966) S-potentials from luminosity units in the retina of fish
669	(Cyprinidae). J Physiol 185:587–599.
670	Nirenberg S, Bomash I, Pillow JW, Victor JD (2010) Heterogeneous response dynamics in
671	retinal ganglion cells: The interplay of predictive coding and adaptation. J Neurophysiol
672	103:3184–3194.
673	Pandarinath C, Victor JD, Nirenberg S (2010) Symmetry breakdown in the ON and OFF
674	pathways of the retina at night: functional implications. J Neurosci 30:10006–10014.
675	Paulsen O, Heggelund P (1994) The quantal size at retinogeniculate synapses determined from
676	spontaneous and evoked EPSCs in guinea-pig thalamic slices. J Physiol 480:505–511.
677	Peichl L (1989) Alpha and delta ganglion cells in the rat retina. J Comp Neurol 286:120–139.

678	Peichl L, Ott H, Boycott BB (1987) Alpha ganglion cells in mammalian retinae. Proc R Soc Lond
679	B 231:169–197.
680	Rathbun DL, Alitto HJ, Warland DK, Usrey WM (2016) Stimulus contrast and retinogeniculate
681	signal processing. Front Neural Circuits 10:1–10.
682	Ratliff CP, Borghuis BG, Kao Y-H, Sterling P, Balasubramanian V (2010) Retina is structured to
683	process an excess of darkness in natural scenes. PNAS 107:17368–17373.
684	Ravi S, Ahn D, Greschner M, Chichilnisky EJ, Field GD (2018) Pathway-specific asymmetries
685	between ON and OFF visual signals. J Neurosci 38:9728–9740.
686	Rieke F (2001) Temporal contrast adaptation in salamander bipolar cells. J Neurosci 21:9445-
687	9454.
688	Sceniak MP, Chatterjee S, Callaway EM (2006) Visual spatial summation in macaque
689	geniculocortical afferents. J Neurophysiol 96:3474–3484.
690	Sceniak MP, Ringach DL, Hawken MJ, Shapley R (1999) Contrast's effect on spatial summation
691	by macaque V1 neurons. Nat Neurosci 2:733–739.
692	Schiller PH (1992) The ON and OFF channels of the visual system. Trends Neurosci 15:86–92.
693	Schiller PH, Logothetis NK (1990) The color-opponent and broad-band channels of the primate
694	visual system. Trends Neurosci 13:392–398.
695	Schiller PH, Sandell JH, Maunsell JHR (1986) Functions of the ON and OFF channels of the
696	visual system. Nature 322:824-825.
697	Shapley RM, Victor JD (1978) The effect of contrast on the transfer properties of cat retinal
698	ganglion cells. J Physiol 285:275–298.
699	Shapley RM, Victor JD (1981) How the contrast gain control modifies the frequency responses
700	of cat retinal ganglion cells. J Physiol 318:161–179.
701	Shushruth S, Ichida JM, Levitt JB, Angelucci A (2009) Comparison of spatial summation
702	properties of neurons in macaque V1 and V2. J Neurophysiol 102:2069–2083.

703	Sillito AM, Cudeiro J, Murphy PC (1993) Orientation sensitive elements in the corticofugal
704	influence on centre-surround interactions in the dorsal lateral geniculate nucleus. Exp Brain
705	Res 93:6–16.
706	Sillito AM, Jones HE (2002) Corticothalamic interactions in the transfer of visual information.
707	Philos Trans R Soc Lond B Biol Sci 357:1739–1752.
708	Solomon SG, Lee BB, Sun H (2006) Suppressive surrounds and contrast gain in magnocellular-
709	pathway retinal ganglion cells of macaque. J Neurosci 26:8715-8726.
710	Solomon SG, White AJR, Martin PR (2002) Extraclassical receptive field properties of
711	parvocellular, magnocellular, and koniocellular cells in the primate lateral geniculate
712	nucleus. J Neurosci 22:338–349.
713	Soto-Sánchez C, Wang X, Vaingankar V, Sommer FT, Hirsch JA (2017) Spatial scale of
714	receptive fields in the visual sector of the cat thalamic reticular nucleus. Nat Commun 8:1-
715	7.
716	Tauchi M, Morigiwa K, Fukuda Y (1992) Morphological comparisons between outer and inner
717	ramifying alpha cells of the albino rat retina. Exp Brain Res 88:67–77.
718	Troy JB, Shou T (2002) The receptive fields of cat retinal ganglion cells in physiological and
719	pathological states: where we are after half a century of research. Prog Retin Eye Res
720	21:263–302.
721	Turner MH, Rieke F (2016) Synaptic rectification controls nonlinear spatial integration of natural
722	visual inputs. Neuron 90:1257–1271.
723	Usrey WM, Alitto HJ (2015) Visual functions of the thalamus. Annu Rev Vis Sci 1:351–371.
724	Usrey WM, Reid RC (2000) Visual physiology of the lateral geniculate nucleus in two species of
725	New World monkey: Saimiri sciureus and Aotus trivirgatis. J Physiol 523:755-769.
726	Vaiceliunaite A, Erisken S, Franzen F, Katzner S, Busse L (2013) Spatial integration in mouse
727	primary visual cortex. I Neurophysiol 110:964–972

728	Vaingankar V, Soto-Sanchez C, Wang X, Sommer FT, Hirsch JA (2012) Neurons in the
729	thalamic reticular nucleus are selective for diverse and complex visual features. Front
730	Integr Neurosci 6:1–17.
731	Victor JD (1987) The dynamics of the cat retinal X cell centre. J Physiol 386:219–246.
732	Wang S, Bickford ME, Horn SC van, Erisir A, Godwin DW, Sherman SM (2001) Synaptic targets
733	of thalamic reticular nucleus terminals in the visual thalamus of the cat. J Comp Neurol
734	440:321–341.
735	Weick M, Demb JB (2011) Delayed-rectifier K channels contribute to contrast adaptation in
736	mammalian retinal ganglion cells. Neuron 71:166-179.
737	Werblin FS, Dowling JE (1969) Organization of the retina of the mudpuppy, Necturus
738	maculosus. II. Intracellular recording. J Neurophysiol 32:339–355.
739	Wilson JR (1989) Synaptic organization of individual neurons in the macaque lateral geniculate
740	nucleus. J Neurosci 9:2931–2953.
741	Zaghloul KA, Boahen K, Demb JB (2003) Different circuits for ON and OFF retinal ganglion cells
742	cause different contrast sensitivities. J Neurosci 23:2645–2654.
743	Zaghloul KA, Manookin MB, Borghuis BG, Boahen K, Demb JB (2007) Functional circuitry for
744	peripheral suppression in Mammalian Y-type retinal ganglion cells. J Neurophysiol
745	97:4327-4340.
746 747	

FIGURE LEGENDS

Figure 1. Stimulus contrast and size affect LGN responses. A, Raster plot of responses (tick marks) from an example LGN (magnocellular) neuron to drifting sinusoidal gratings varying in stimulus diameter (rows) and stimulus contrast (panels) across time. **B**, Area summation responses for the same neuron at different stimulus contrasts fit with a difference of Gaussian function indicated with solid lines. Closed circles and error bars represent the mean ± SEM. **C**, Illustration of area summation response curve and parameters of interest. **D-F** Peak response, optimal size, and suppression index measured at 3 levels of contrast for the example LGN neuron.

Figure 2. Contrast dependence of spatial integration. A, Scatter plot of the suppression index at high and low contrast conditions across our sample of LGN neurons (n = 75). The distributions are histograms of suppression index values at high contrast and low contrast, the dashed lines indicate the mean for each contrast condition. **B,** Scatter plot of the optimal size at high and low contrast conditions across our sample of LGN neurons (n = 75). The distributions are histograms of optimal size values at high contrast and low contrast, the dashed lines indicate the mean for each contrast condition.

Figure 3. Variations in how cells respond to changes in stimulus contrast. A, Contrast response function for an example LGN magnocellular neuron. B, Contrast response function for an example LGN parvocellular neuron. Solid lines indicate the hyperbolic ratio function fit. Closed circles and error bars indicate the mean \pm SEM. Dotted lines indicate the contrast to evoke a half-maximum response (C_{50}).

Figure 4. Influence of contrast on suppression and size preferences of cells in the magnocellular and parvocellular pathways. A, Box plots showing the distribution of suppression index values under high and low contrast conditions for magnocellular cells (n = 35) and parvocellular cells (n = 19). The red horizontal lines within each box represent the median values, and the notches indicate the 95% confidence interval for the median. Edges of the boxes represent the 25th and 75th percentiles, and the whisker bars extending beyond the box correspond to the data range, excluding outlying data points that are shown individually (red crosses). Superimposed circles and error bars indicate the mean ± SEM. B, Scatter plot of the suppression index at high and low contrast conditions for magnocellular cells, indicating an increase in suppression strength at high contrast as shown by the data above the unity line. C, Scatter plot of the suppression index at high and low contrast conditions for parvocellular cells. D, Distributions of contrast-dependent changes in the suppression index for magnocellular cells and parvocellular cells. E, Distributions of optimal size values under high and low contrast conditions for magnocellular cells (n = 35) and parvocellular cells (n = 19). F, Scatter plot of the optimal stimulus size at high and low contrast conditions for magnocellular cells, indicating an increase in the optimal size at low contrast as shown by the data below the unity line. G. Scatter plot of the optimal size at high and low contrast conditions for parvocellular cells. H, Distributions of contrast-dependent changes in optimal size (bounded index, see Materials and Methods) for magnocellular cells and parvocellular cells.

791

792

793

794

795

796

797

772

773

774

775

776

777

778

779

780

781

782

783

784

785

786

787

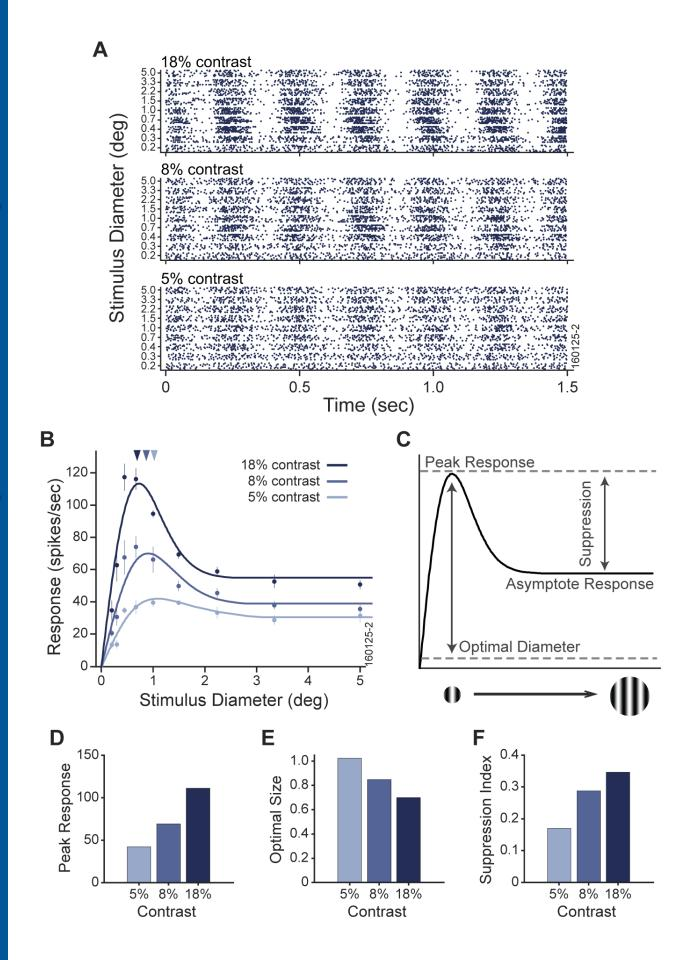
788

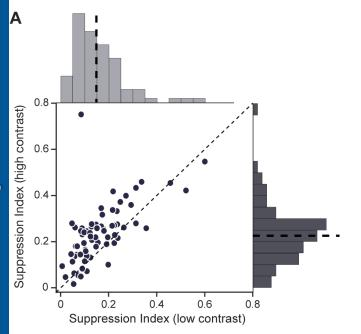
789

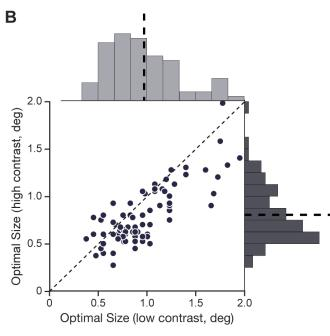
790

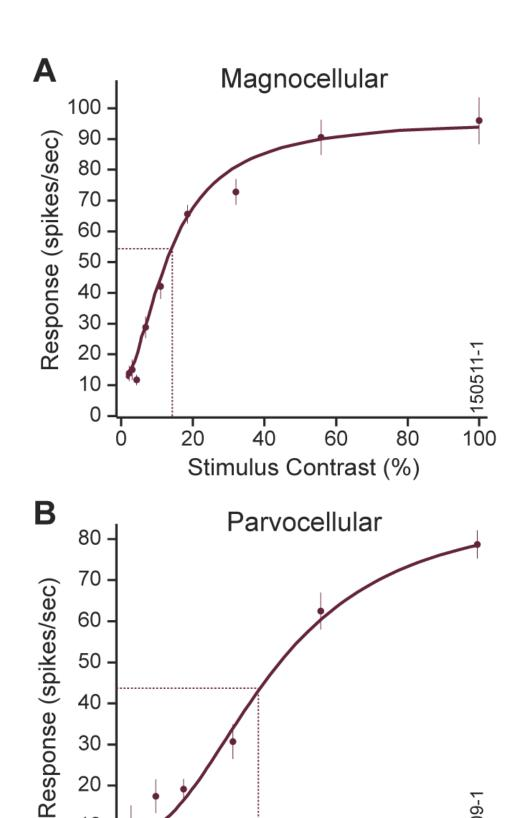
Figure 5. Asymmetries in suppression and size preference ON and OFF cells in the magnocellular pathway. **A**, Box plots showing the distribution of suppression index values under high and low contrast conditions for magnocellular OFF cells (*n* = 19) and ON cells (*n* = 16). Box plot conventions as described for Figure 4A. **B**, Scatter plot of the suppression index at high and low contrast conditions for magnocellular OFF and ON cells. **C**, Distributions of contrast-dependent changes in the suppression index for magnocellular OFF cells and ON cells.

${f D}$, Distributions of optimal size values under high and low contrast conditions for magnocellular
OFF cells ($n = 19$) and ON cells ($n = 16$). E, Scatter plot of the optimal size at high and low
contrast conditions for magnocellular OFF cells and ON cells. F, Distributions of contrast-
dependent changes in optimal size (bounded index, see Materials and Methods) for
magnocellular OFF cells and ON cells.
Figure 6. Optimal size as a function of eccentricity for OFF and ON cells in the
magnocellular pathway. Scatter plot of the optimal size pooled across conditions of high and
low contrast against eccentricity, illustrating a significant positive correlation for both
magnocellular OFF cells and ON cells.
Figure 7. Functional asymmetries in forms of gain control across cells in the
magnocellular pathway. A, Scatter plot of the suppression index against optimal size pooled
across conditions of high and low contrast. ${f B}$, Distributions of the C_{50} for magnocellular OFF
cells ($n = 19$) and ON cells ($n = 16$). C , Scatter plot of the suppression index pooled across
conditions of high and low contrast against the C_{50} .









Stimulus Contrast (%)

0-151109-1

